Cardiac Motion Recovery and Boundary Conditions Estimation by Coupling an Electromechanical Model and Cine-MRI Data

Florence Billet, Maxime Sermesant, Hervé Delingette, Nicholas Ayache

Cardiac Motion Recovery and Boundary Conditions Estimation by Coupling an Electromechanical Model and Cine-MRI Data

Florence Billet, Maxime Sermesant, Hervé Delingette, and Nicholas Ayache

INRIA Sophia-Antipolis, 2004 route des lucioles - BP 93, FR-06902 Sophia Antipolis, France. Corresponding author: florence.billet@inria.fr

Abstract. We present a method for cardiac motion recovery using the adjustment of an electromechanical model of the heart to cine MRI. This approach is based on a proactive model which consists in a constrained minimisation of an energy coupling the model and the data. The presented method relies on specific image features in order to constrain the motion of the endocardia and epicardium and impose boundary conditions at the base. Thus, image intensity and gradient information are used to constrain the motion of the myocardium surfaces while a 3D block matching technique leads to the motion estimation of base vertices. Finally, we show that the implicit time integration of those forces and personalised boundary conditions lead to a better cardiac motion recovery from cine-MR images.

1 Introduction

Cardiovascular diseases are the number one cause of death in the industrialised world and is projected to remain so. That's why the modeling of the heart's electromechanical activity is an active research area [1–3]. Moreover, the coupling of these models and clinical data allows us to personalise them and then to simulate a number of pathologies or the effect of therapeutic actions, and to analyse the cardiac function of the considered patient.

There exist several approaches in the literature to create such patient-specific models of the heart from clinical images. The concept of deformable models is often used to adjust a geometrical model of the heart on time series of medical images [4–6]. In such approaches, the surface or the volumetric mesh is fitted to the apparent boundaries of the heart in the image by minimising the sum of an image energy and a regularising or internal energy. Those models may produce proper segmentations and are rather efficient, however they rely on little *a priori* knowledge of the heart motion which limits their ability to recover tangential motion due to the aperture problem.

Other approaches strongly constrain the estimation of motion by coupling an electromechanical heart model using data assimilation methods. In such a framework, dynamical systems representing electromechanical models of the heart are adjusted to time series of images by adding a filter that constrain the state variables (*i.e* the position and the velocity) and the model parameters to match the

available observations. P.C Shi *et al.* introduced such techniques by integrating cardiac models and Kalman filters [7, 8]. However, the use of extended Kalman filtering is often limited since they implies the use of full covariance matrices whose size are equal to the square of the number of state variables augmented by the number of parameters to estimate. To avoid the curse of dimensionality, some authors [9] have devised non optimal filters which do not involve any matrix inversion (unlike Kalman filtering). This approach leads to much faster computations and has been the inspiration of the work presented in this paper.

We showed in [14] the equivalence under some hypothesis between the method proposed in [9] and the use of a proactive deformable model introduced in [13]. In this paper, we use the proactive deformable model which extends the concept of deformable models by adding an active electromechanical model of the heart motion as the regularising energy term. In this paper, we improve from our previous work with two additional contributions. First, we provide an implicit formulation of image forces that can better predict the image forces between two time steps. Second, we estimate the motion of the base of the ventricles, where the ventricles are connected to the atria and outflow tracts. This represents a significant advance since most previous work on electromechanical modelling of the heart consider that ventricle bases are fixed or linked to fixed points through springs. To recover the base motion from image, we use a block matching technique at the base points that uses intensity correlation to track points along the cardiac cycle.

2 Electromechanical Model

As we want the complexity of the model to match the relatively sparse measures available from imaging data, we consider in this paper a fairly reduced electromechanical model. For instance, our model relies on linear elasticity for myocardium mechanics although a nonlinear material undergoing large strain would be better suited. However, we found the current reduced model to be a good trade-off in terms of computational efficiency and physiological realism. Furthermore, this coarse level of modeling makes the estimation of the mechanical state and parameters tractable and allows us to test the behaviour of the model on several heart beats. Our cardiac model couples two biophysical components : electrophysiology and biomechanics. Due to its efficiency, we use a multi-front anisotropic Eikonal approach solved with a Fast Marching algorithm on a volumetric tetrahedral mesh [10].

The depolarisation time t_d of the electrical wave for a given vertex of the volumetric mesh is computed by solving the anisotropic Eikonal equation $v^2(\nabla t_d^T D \nabla t_d) = 1$, where v is the local conduction velocity parameter and D is the tensor defining the conduction anisotropy. In the fibre coordinates, $D = diag(1, \rho, \rho)$, where ρ is the conduction anisotropy ratio between longitudinal and transverse directions.

The biomechanical model, derived from a multi-scale modelling of the myocardium detailed in [11], is composed of an active contractile element controlled

by the electrophysiology and a parallel one which represents the properties of the tissue and is anisotropic linear visco-elastic.

The active contractile element is controlled by the depolarisation time t_d computed with the Eikonal equation and creates a stress tensor $\sigma_C \boldsymbol{f} \otimes \boldsymbol{f}$ where $\boldsymbol{f}$ is the 3D fibre orientation, $\otimes$ the dyadic product and σ_C the strength of the contraction defined by the equation 1:

$$\sigma_C(t) = \begin{cases} \sigma_0 \left(1 - e^{k_{ATP}(t_d - t)}\right) & \text{during depolarisation } t_d \leq t < t_r \\ \sigma_C(t_r) e^{k_{RS}(t_r - t)} & \text{during repolarisation } t_r \leq t < t_d + HP \end{cases} \quad (1)$$

where $t_r = t_d + APD$ is the repolarisation time with APD the active potential duration, σ_0 the maximum of the contraction, k_{ATP} and k_{RS} the contraction and relaxation rates respectively and HP the heart period. This tensor results in a 3D contraction force $\boldsymbol{f}_C$ for each vertex of each element.

Finally, the simplified dynamic law is: $M\ddot{Y} + C\dot{Y} + KY = F_{PV} + F_C + F_B$ where M, C are the mass, Rayleigh damping matrices, K the stiffness matrix, F_C, F_PV, F_B the force vectors respectively created by the active contractile elements, corresponding to the pressure forces in the ventricles and corresponding to other boundary conditions and Y, $\dot{Y} = dY/dt$, $\ddot{Y} = d^2Y/dt^2$ respectively the position, velocity and acceleration.

The four cardiac cycles (filling, isovolumetric contraction, ejection, isovolumetric relaxation) were simulated as presented in [13]. We compute the arterial pressures using a 3-element Windkessel model described in [12].

The pressure forces are computed differently in the cardiac phases. In the filling phase, they are set to the values of the pressures in the atrias. In the ejection phase, they are set to the arterial pressures computed with the 3-element Windkessel model. In the isovolumetric phases, the ventricular pressures are computed in order to counterbalance the contraction forces and to keep the ventricle volumes constant.

3 Cine MR Image Processing

Cine-MRI data consists in a sequence of 20 to 30 high resolution MR images of the heart that describes a whole cardiac cycle. We build a myocardium mesh that fits the mid-diastolic MRI image of the sequence when the filling of the ventricles is almost finished, just before the atrial contraction. As described in [14], we select this mid-diastole image based on blood pool volumes curves. Then, an interactive tool is used to delineate the epicardium and left and right ventricles endocardia in order to create three binary masks of the epicardium and the endocardia. We combined these masks to obtain the binary mask of the myocardium and create the mesh with an isosurface extraction and tetrahedral mesh generation.

Furthermore, synthetic fibre orientations are computed by linearly interpolating the elevation angle between the fibre and the short axis plane, from 80^o on the endocardium to -80^o on the epicardium.

4 Proactive Deformable Model

4.1 Image Forces

In deformable model approaches, the optimal shape corresponds to the minimization of the sum of an image energy and a regularizing energy. The use of an electromechanical model as a regularising term allows us to introduce some *a priori* knowledge about the active cardiac motion and thus to recover some movement (like the tangential motion) which cannot be obtained from classical geometrical tracking methods. Thus, we add to the previous dynamic equation $M\ddot{Y} + C\dot{Y} + KY = F_{PV} + F_C + F_B$ an image force F_{img} that derives from an image energy.

Of course, the image forces have no physiological meaning, and then the estimated motion is not physiological. But by coupling the model and the data and by estimating the model parameters (which is the next step of this work), the motion generated by the model should converge to the one observed in the images. Thus, the intensity of image forces should decrease along the estimation and the estimated motion should be more and more physiological.

The image energy is a metric that compares the simulated motion and the observed one. Thus, for each vertex Y_i of the epicardium or endocardium surfaces, if we define as Z_i the closest point on the apparent image boundary along the normal direction N_i at Y_i, then the image force at Y_i is $F_{img} = 2\gamma_i(Z_i - Y_i)$ (see [14, 13]). In this equation γ_i is the image gain that depends on the confidence we have in the corresponding image point Z_i. In fact, with high gains, the estimated state will rely more on image data information than in the electromechanical model. Conversely, with gains equal to 0, the estimation does not take into account the data and is equivalent to the electromechanical model alone. Thus, the choice of the gains depends on the relative confidence in the model and the data. Furthermore, we showed in [14] how to set these gains in order to ensure convergence. For each vertex Y_i of the epicardium or endocardium surfaces, the definition of Z_i is a function of the image intensity and image gradient. More precisely, as shown in Fig. 1 (a) and (b), we first extract the intensity profile at Y_i along N_i and then determine the closest voxel Z_i whose image gradient norm is greater than a threshold and whose intensity is within a given range value. Those threshold and range value are set on the first image and kept constant during the cardiac cycle. In Fig. 1 (a) and (b), the way to find the point Z_i is shown in 2D for more simplicity, but it is performed using the all 3D image.

4.2 Implicit Image Forces

The image forces then may be temporally integrated either with an explicit or implicit scheme. In [14], we used an explicit scheme for time integration. Thus, at each time step t, we solved the approximated equilibrium equation $\tilde{K}Y^{t+dt} = F + F^t_{img}$ to compute the position Y^{t+dt} of the mesh at the following time step, where $\tilde{K}$ is the generalised stiffness matrix, F the external physical forces and F^t_{img} the image force as $2\gamma_i(Z^t_i - Y^t_i)$ if Y_i belongs to the heart surfaces

and 0 otherwise. As we know the position of the mesh at time t, we could find the point Z_i^t as explained above. This explicit scheme is computationally efficient since the generalised stiffness matrix does not change other time. However with such scheme, the proactive deformable model tends to lag behind the image observation which introduces a bias especially for large time steps.

Therefore, in this paper, we introduce an implicit scheme solving $\tilde{K}Y^{t+dt} = F + F_{img}^{t+dt}$, which requires predicting the next image force F_{img}^{t+dt}. To this end, we use a Taylor expansion of the image point Z_i^{t+dt}:

$$Z_i^{t+dt} = Z_i^t + \left(\frac{\partial Z_i}{\partial Y_i}\right)^t (Y_i^{t+dt} - Y_i^t) = Z_i^t + B(Y_i^{t+dt} - Y_i^t) \tag{2}$$

The B matrix is a 3×3 matrix that indicates how point Z_i moves as a function of Y_i. We provide here a first order approximation of this matrix by discarding the effect of surface curvature. Thus, we consider that Y_i lies on a plane with normal N_i while Z_i lies on a plane oriented by normal N_i^{img}. With those hypotheses, upon a displacement dY_i, Z_i is determined as the intersection of the line passing through $Y_i + dY_i$ and directed by N_i through the plane P_i^{img}. Obviously, only components of dY_i orthogonal to N_i entails a change in the point Z_i. Similarly, only components orthogonal to N_i^{img} would entail a change in point Z_i. Thus, skipping a detailed proof, one can show that the matrix B can be written as :

$$B = \frac{1}{cos^2\beta}(I_{3\times3} - N_i^{img} \otimes N_i^{img})(I_{3\times3} - N_i \otimes N_i) \tag{3}$$

where β is the angle between N_i and N_i^{img}, $I_{3\times3}$ is the identity matrix and $a \otimes b = ab^T$ is the dyadic product between the vectors a and b.

Finally, we need to solve the following equation: $(\tilde{K} + K_{img})Y^{t+dt} = F + \tilde{F}_{img}$ with $\tilde{F}_{img}$ a vector of size $3 \times N$ whose 3D component $\tilde{\boldsymbol{f}}_{img,i}$ is equal to $2\gamma_i(Z_i^t - Y_i^t) + 2\gamma_i(I_{3\times3} - B)Y_i^t$ if Y_i belongs to the myocardium surfaces, and 0 otherwise and with K_{img} a block diagonal matrix whose 3×3 component $(K_{img})_i$ is equal to $2\gamma_i(I_{3\times3} - B)$ if Y_i belongs to the myocardium surfaces, and the null matrix otherwise.

5 Boundary Constraints Estimation

Due to the modeling of the electromechanical behaviour of the heart, we have a lot of *a priori* knowledge on the motion of the ventricles. But for the base of the ventricles, near the atria, we have little *a priori* knowledge of the motion, and boundary constraints are set simply by attaching base vertices to fixed springs. Thus, we introduce here a way to estimate these boundary constraints by using a more complex external energy.

We cannot rely on intensity profiles to find Z_i as described in the previous section. Indeed this would only estimate displacement of base vertices along its normal direction which is ill-defined and physically incorrect. Instead, we use a 3D search method based on 3D block matching algorithm, as in [15]. We hope

therefore to better recover the real motion of the base, and not only its apparent one. Finally, we can use the similarity measure between the image blocks as a way to control the confidence in the point Z_i.

Therefore, we attach to each base vertex of the initial mesh a surrounding block of voxels from the reference image, which is the first image of the simulation (see section 3). Then, we search at each time step the most similar block around the current position in the following image of the cardiac cycle (the target image) (see Fig. 1 (c) and (d)). This is based on the assumption that the intensity around a given vertex of the base of the mesh should be similar in the two images, the difference coming from noise and from the movement of the vertex between the two images, which is not very important at the base of the heart, near the valve. The matching voxel selected is the center of the block in the target image maximising the chosen similarity criterion. Then, in order to take into account that the motion at the base is mainly a vertical one, we project the vector connecting the current point and the marching voxel on the normal of the mesh at this current point. The external force is then proportional to the norm of this projection and directed from the normal of the mesh at the considered point. The search range and the search step can be changed in a coarse to fine approach, as in [15]. In this paper, we used a similarity based on the sum of square differences, but several other similarity measures can be used depending of the noise and the used image modalities. Moreover, these estimated boundary constraints could be set as inputs in further simulations with the personalised model.

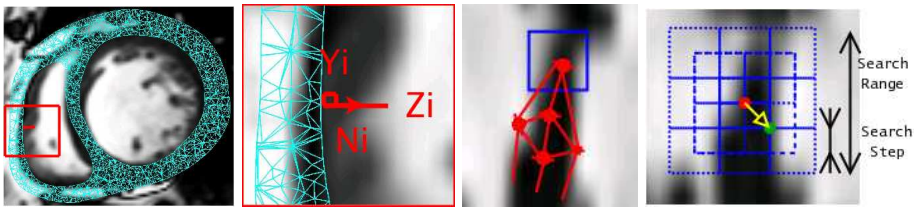

Fig. 1. (a, b) Surface image forces and corresponding Z_i point in the image. (c,d) Block matching algorithm (c) Reference image: initialisation in the reference image of the 3D block. (d) Target image: most similar block search around the current position.

6 Results

6.1 Validation on Synthetic Data

We generated synthetic cine-MR images using the electromechanical model with standard values. We considered 29 instants of the second simulated cycle and

we generated the corresponding segmented 3D images, using tetrahedra rasterisation. We use for the different state estimation a cardiac model with same parameters as the model used to generate the synthetic data except for the reference position and the damping value.

We choose to estimate the state using a low damping because the effect of the implicit forces is more visible with low damped systems. Indeed in a highly damped system all applied forces are smoothed to a large extent which entails a delay in the reaction of the cardiac model to new image information.

We then compare the state vector estimation (position and velocity) with no image forces and with an explicit and implicit time integration of image forces. The gain γ of the image forces is set to the same value for the two estimations. For each method, we computed the root mean squared error (RMSE) between the estimated positions and the positions of the reference simulation (see Fig. 2 (a)). The RMSE with implicit forces is lower than the one with explicit forces (15% lower), and much lower than the one computed without image forces. Indeed, the average of all RMSE without image forces, with explicit and implicit image forces are respectively 14.9mm, 4.5mm and 3.6mm. Furthermore, explicit integration with low damping leads to large oscillation in the right ventricle (see Fig.2 (b)) due to undamped high frequencies in image forces. Finally, we can see that the mesh obtained with implicit forces better fits the segmented contour than the mesh obtained with explicit forces.

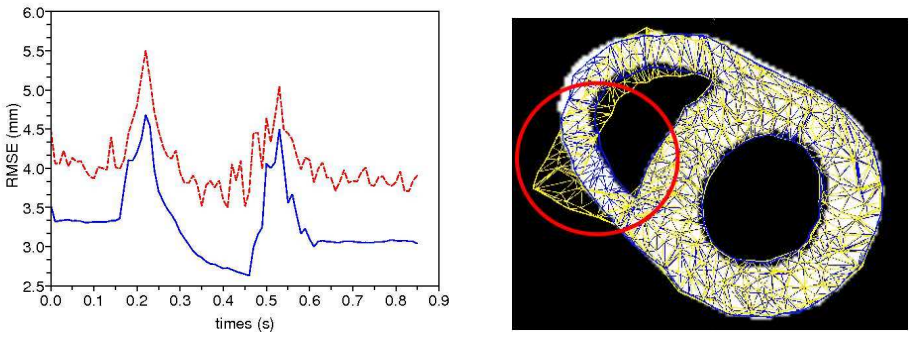

(a) (b)

Fig. 2. (a) RMSE between the positions of the reference simulation and the positions estimated with implicit forces (solid) and explicit forces (dashed). (b) Image and superimposed meshes estimated with implicit (blue) and explicit (yellow) image forces.

6.2 Results on Clinical Data

We used cine-MRI data of a patient with a left bundle branch block (LBBB) to test the effect of the block matching forces. The sequence consists in 30 images

that describe a total heart cycle. The resolution of this dataset is $1.56 \times 1.56 \times 10\text{mm}^3$. In order to increase the robustness of the algorithms on clinical routine cardiac MRI, images are pre-processed. First, images are trilinearly resampled to get isometric voxel spacing (and then the resolution becomes $1.56 \times 1.56 \times 1.56\text{mm}^3$). Next, the contrast is enhanced by removing the extrema quantiles of the grey-level histogram. Finally, the histogram is linearly rescaled between 0 and 255 to have consistent intensities between images.

We manually adjusted the electrical parameters using the ECG and, in this case, with some clinically measured propagation times of the patient. If we have no measures of this propagation times, we initialize the electrical model with the volumes curves extracted from the images, as shown in [14]. The passive mechanical parameters used are taken from the literature [7]. In order to calibrate the active mechanical parameters, we use the volume curve to compute the ejection fractions, wich are closely related to these parameters. For our data, σ_0 was set to 0.09 MPa/mm^2 for the left ventricle, 0.07 MPa for the right ventricle and 0.06 for the scars. The cardiac cycle duration is 1.035s.

We did three different estimations, all using the implicit forces described above for the epicardium and the endocardium surfaces. The first estimation uses no image forces applied to the base and no boundary constraints. The second one uses no image forces applied to the base, but applies boundary constraints involving fixed springs. The last one applies block matching forces on the base and image forces in the endocardium and epicardium surfaces.

Fig. 3 shows some short and long axis views with the contours of the three estimated positions superimposed with the corresponding MR image.

With no boundary constraints and no image forces there is no attach points in the model of the heart which entails that the generalised stiffness matrix may become singular. Also we have no *a priori* knowledge of the base motion. Thus, large errors in the estimation may occur, as shown in Fig. 3 (d, e and f) (the motion of left part of the left ventricle and of the top of the right ventricle is not well recovered).

With boundary constraints on the base, the model may be too much constrained, specially during the contraction as shown in Fig. 3 (c and d). For instance, the motions of the septum (see the short axis views of Fig. 3 (c and d)) and at the top of the lateral part of the right ventricle (see the long axis views of Fig. 3 (c and d)) are not well recovered.

Finally, the block matching forces achieve a good compromise between these two approaches. The motion of the base vertices are determined by block matching instead of being fixed with springs. We can see that the right ventricle motion has been well recovered, even during the contraction of the heart, as shown in Fig. 3 (b, c and d). However, we can see that the motion of the top of the septum is not well recovered, due to a not so good intitial segmentation of the top of the septum. This segmentation error makes the initialisation of the block matching algorithm not good, and then, the founded appariements try to keep this error. We can see here the need of a good segmentation for the use of the block matching approach.

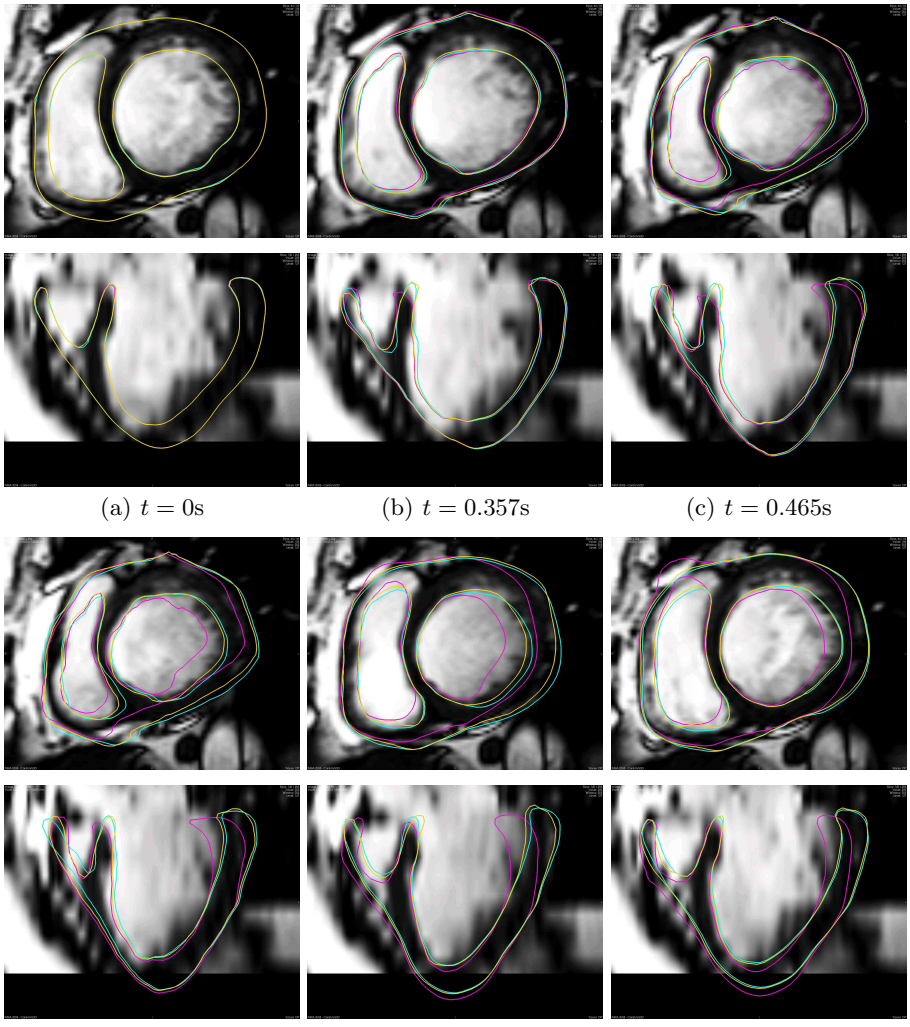

(a) $t = 0$s (b) $t = 0.357$s (c) $t = 0.465$s

(d) $t = 0.574$s (e) $t = 0.743$s (f) $t = 0.961$s

Fig. 3. MR image short axis (top) and long axis (bottom) slices at different times of the heart cycle, with the contrours of the estimated model position without boundary constraints (magenta), with boundary constraints (cyan) and with a block matching algorithm (yellow)

7 Conclusion

We presented a method which relies on specific image features to recover the motion of the myocardium and estimate boundary constraints at the base. The use of implicit time integration of image forces allows us to ensure a better accuracy and smoother motion tracking for low damped systems. Furthermore, the use of

a 3D block matching algorithm for the estimation of the boundary constraints at the base appears to be a good trade off between cardiac motion recovery with no boundary constraints and with classical boundary constraints consisting of fixed vertices or fixed springs and set manually. Finally, these promising results must be extended in order to perform parameter estimation of the model which would lead to a patient-specific electromechanical model of the heart.

Acknowledgements: INRIA Research Action CardioSense3D, European project euHeart (FP7/2007-2013 no 224495), Microsoft Research.

References

1. Hunter, P.J., Nash, M.P., Sands, G.B.: Computational Electromechanics of the Heart. In: Computational biology of the heart, pp. 345–407. (1997)
2. Sachse, F., Seemann G., Werner, C., Riedel, C., Dössel, O.: Electro-mechanical modeling of the myocardium: Coupling and feedback mechanisms. In: Proc. Comp. Cardiol. 28, pp. 161–164, (2001)
3. Frangi, A., Niessen, W., Viergever, M.: Three-Dimensional Modeling for Functional Analysis of Cardiac Images: A Review. IEEE Trans. on Med. Im. 1, 2–25 (2001)
4. Papademetris, X., Sinusas, A. J., Dione, D. P., Duncan, J. S.: 3D Cardiac Deformation from Ultrasound Images. In: MICCAI 1679, pp. 420–429 (1999)
5. Montagnat, J., Delingette, H.: 4D Deformable Models with temporal constraints: application to 4D cardiac image segmentation. Med. Im. Anal, 9, 87–100 (2005)
6. Qian, Z., Metaxas, D. , Axel, L.: A Learning Framework for the Automatic and Accurate Segmentation of Cardiac Tagged MRI Images. In: Comp. Vis. for Bio. Im. App., pp. 93–102 (2005)
7. Shi, P., Liu, H.: Stochastic finite element framework for simultaneous estimation of cardiac kinematic functions and material parameters. Med. Im. An. 7, 445–464 (2003)
8. Wong, K. C. L., Zhang, H., Liu, H., Shi, P.: Physiome Model Based State-Space Framework for Cardiac Kinematics Recovery. In: MICCAI, pp. 720–727 (2006)
9. Moireau, P., Chapelle, D., Le Tallec, P.: Joint state and parameter estimation for distributed mechanical systems. Computer Methods in Applied Mechanics and Engineering 197, 659–677 (2008)
10. Sermesant, M., Konukoglu, E., Delingette, H. Coudiere Y., Chinchaptanam, P., Rhode K. S., Razavi R., Ayache, N.: An anisotropic multi-front fast marching method for real-time simulation of cardiac electrophysiology. In: FIMH 4466, pp. 160–169 (2007)
11. Bestel, J., Clément, F., Sorine M.: A Biomechanical Model of Muscle Contraction. In: MICCAI 2208, pp. 1159–1161 (2001)
12. Stergiopulos, N., Westerhof, B., Westerhof, N.: Total arterial inertance as the fourth element of the windkessel model. Am. J. of Phys. 276, H81-8 (1999)
13. Sermesant, M., Delingette, H., Ayache, N.: An Electromechanical Model of the Heart for Image Analysis and Simulation. IEEE TMI 25, 612–625 (2006)
14. Billet, F., Sermesant, M., Delingette, H., Ayache, N.: Cardiac Motion Recovery by Coupling an Electromechanical Model and Cine-MRI Data: First Steps. In: Proc. of the Workshop on Comp. Biom. Med. MICCAI (2008)
15. Ourselin, S. and Roche, A. and Prima, S. and Ayache, N.: Block Matching: A General Framework to Improve Robustness of Rigid Registration of Medical Images. In: MICCAI 1935, pp 557–566 (2000)